

# Second-order topological insulator in a coinless discrete-time quantum walk

Ya Meng,<sup>1</sup> Gang Chen,<sup>1,2,3,\*</sup> and Suotang Jia<sup>1,2</sup>

<sup>1</sup>*State Key Laboratory of Quantum Optics and Quantum Optics Devices,  
Institute of Laser Spectroscopy, Shanxi University, Taiyuan 030006, China*

<sup>2</sup>*Collaborative Innovation Center of Extreme Optics,  
Shanxi University, Taiyuan, Shanxi 030006, China*

<sup>3</sup>*Collaborative Innovation Center of Light Manipulations and Applications,  
Shandong Normal University, Jinan 250358, China*

Higher-order topological insulators not only exhibit exotic bulk-boundary correspondence principle, but also have an important application in quantum computing. However, they have never been achieved in quantum walk. In this paper, we construct a two-dimensional coinless discrete-time quantum walk to simulate second-order topological insulator with zero-dimensional corner states. We show that both of the corner and edge states can be observed through the probability distribution of the walker after multi-step discrete-time quantum walks. Furthermore, we demonstrate the robustness of the topological corner states by introducing the static disorder. Finally, we propose a possible experimental implementation to realize this discrete-time quantum walk in a three-dimensional integrated photonic circuits. Our work offers a new route to explore exotic higher-order topological matters using discrete-time quantum walks.

## I. INTRODUCTION

Quantum walk, which describes the propagation of quantum particles on a lattice [1–3], is a quantum version of classical random walk. Due to its simplicity and high controllability, quantum walk has become a powerful tool for universal quantum computing [4, 5] and quantum simulation [6–9]. Inspired by an original theoretical paper of Kitagawa [10], discrete-time quantum walk (DTQW) has become an outstanding platform for simulating various topological phenomena [11–19]. In particular, the topological edge states and winding numbers have been detected by both unitary [20–26] and non-unitary [27–31] one-dimensional DTQWs. For the two-dimensional case, the one-dimensional edge states have been observed without [32, 33] and with [34] the synthetic gauge field. Very recently, the Chern number has been successfully probed by an anomalous displacement [35].

Notice that the current research on topological features of DTQWs only focus on the simulation of the first-order topological insulator, which supports topological protected states in the  $(d - 1)$ -dimensional boundaries for a  $d$ -dimension system. Recently, higher-order topological insulators, which have lower-dimensional gapless boundary states, have attracted much attention in both theory [36–40] and experiment [41–46]. Physically, these higher-order topological insulators exhibit an exotic bulk-boundary correspondence principle that an  $n$ th-order topological insulator supports gapless  $(d - n)$ -dimensional boundary states. Moreover, these gapless boundary states can support nontrivial fractional quasiparticles (such as parafermion or Ising anyon etc.), providing a new architecture for quantum information processing and quantum computing [47, 48]. Nevertheless,

these interesting higher-order topological phases have never been achieved in quantum walks.

In this paper, we introduce a two-dimensional coinless DTQW to simulate a second-order topological insulator, which hosts the zero-dimensional corner states and one-dimensional edge states. We show that both of the corner and edge states can be observed through the probability distribution of the walker after multi-step DTQWs. Furthermore, we demonstrate the robustness of the topological corner states by introducing the static disorder. Finally, we propose a possible experimental implementation in a three-dimensional integrated photonic circuits. Since the coupling and phase between each two lattice sites at each step of DTQWs can be adjusted independently, our proposal can be extended directly to realize other exotic higher-order topological insulators, such as the non-Hermitian [49–51] and Floquet higher-order topological insulators [52–56], which have not been observed in experiments. Our work offers a new route to explore exotic topological matters using DTQWs.

This paper is organized as follows. In Sec. II, we introduce a two-dimensional coinless DTQW. In Sec. III, we demonstrate the existence of the zero-dimensional corner states and the one-dimensional edge states through calculating the spectra and the topological invariant. In Sec. IV, we show the probability distributions of the walker after multiple-step DTQWs. We also verify the robustness of the corner states by introducing the static disorder. In Sec. V, we propose a possible experimental implementation in a three-dimensional integrated photonic circuits. Finally, we give the summarization in Sec. VI.

---

\*Electronic address: [chengang971@163.com](mailto:chengang971@163.com)

## II. A TWO-DIMENSIONAL COINLESS DTQW

We begin to introduce a two-dimensional SSH model with  $\pi$ -flux per plaquette, which is governed by the Hamiltonian

$$H = \sum_{x,y} (t_x a_{x+1,y}^\dagger a_{x,y} + t_y e^{ix\pi} a_{x,y+1}^\dagger a_{x,y}) + \text{H.c.}, \quad (1)$$

where  $a_{x,y}^\dagger$  ( $a_{x,y}$ ) is the creation (annihilation) operator of a spinless particle at the site  $(x,y)$ ,  $t_{x(y)} = t + (-1)^{x(y)}\delta t$  are the two types of hopping amplitudes in the  $x$  ( $y$ ) direction, respectively, and can be defined as  $J_1 = t - \delta t$ ,  $J_2 = t + \delta t$ , and H.c. is the Hermitian conjugate. This Hamiltonian can host the topological-protected corner states [36, 37]. In the following, we will construct a two-dimensional coinless DTQW to simulate the second-order topological insulator, based on the Hamiltonian (1).

We firstly divide it into four parts

$$H = H_{2y} + H_{1y} + H_{2x} + H_{1x}, \quad (2)$$

where  $H_{1x}$  ( $H_{2x}$ ) and  $H_{1y}$  ( $H_{2y}$ ) are the intracellular (intercellular) hoppings along the  $x$  and  $y$  directions, respectively. Then, we construct a one-step operator of a DTQW as

$$\begin{aligned} U_{\text{step}} &= e^{-i\frac{\pi}{4}\frac{H_{2y}\Delta T}{\hbar}} e^{-i\frac{\pi}{4}\frac{H_{1y}\Delta T}{\hbar}} e^{-i\frac{\pi}{4}\frac{H_{2x}\Delta T}{\hbar}} e^{-i\frac{\pi}{4}\frac{H_{1x}\Delta T}{\hbar}} \\ &= U_4 U_3 U_2 U_1. \end{aligned} \quad (3)$$

For simplicity, we use the units  $\Delta T = \hbar = 1$  hereafter. For the Hamiltonian (1), these four substep operators are chosen as

$$U_1 = \sum_{x=0}^{M/2-1} V_{2x+1} \otimes \mathcal{I}_y, \quad (4)$$

$$U_2 = (|1\rangle_x \langle 1| + |M\rangle_x \langle M|) \otimes \mathcal{I}_y + \sum_{x=1}^{M/2-1} V_{2x} \otimes \mathcal{I}_y, \quad (5)$$

$$U_3 = \sum_{x=1}^M \sum_{y=0}^{M/2-1} |x\rangle \langle x| \otimes V_{2y+1}, \quad (6)$$

$$\begin{aligned} U_4 &= \mathcal{I}_x \otimes (|1\rangle_y \langle 1| + |M\rangle_y \langle M|) \\ &+ \sum_{x=1}^M \sum_{y=1}^{M/2-1} |x\rangle \langle x| \otimes V_{2y}, \end{aligned} \quad (7)$$

where the translation operators in the  $x$  and  $y$  directions are defined as

$$V_x = \cos\left(\frac{\pi}{4}r\right) [|x\rangle \langle x| + |x+1\rangle \langle x+1|] - i \sin\left(\frac{\pi}{4}r\right) [|x+1\rangle \langle x| + |x\rangle \langle x+1|], \quad (8)$$

$$V_y = \cos\left(\frac{\pi}{4}r\right) [|y\rangle \langle y| + |y+1\rangle \langle y+1|] - i \sin\left(\frac{\pi}{4}r\right) [e^{ix\pi} |y+1\rangle \langle y| + e^{-ix\pi} |y\rangle \langle y+1|]. \quad (9)$$

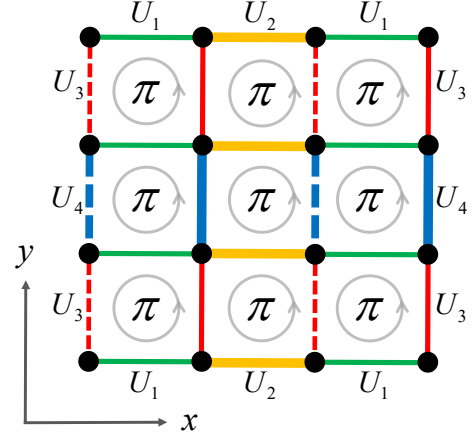


FIG. 1: The proposed implementation of a coinless DTQW in a two-dimensional lattice. The links of the lattice are marked with different colors, degrees of thickness, and linetypes, respectively. The different colors represent four substep operators  $U_i$  in Eqs. (4)-(7), respectively. The links with the different thicknesses represent two types of hopping amplitudes  $J_1$  and  $J_2$ , respectively. The dashed lines in the  $y$  direction indicate the required  $\pm\pi$  phases of the hopping amplitudes, which can induce a  $\pi$ -flux when a walker goes through a elementary cell anticlockwise.

This DTQW is implemented in the Hilbert space  $|x\rangle \otimes |y\rangle$ , with  $x \in \{1, M\}$  and  $y \in \{1, M\}$  ( $M$  is even). The operator  $\mathcal{I}_{x(y)}$  denotes a  $M \times M$  identity matrix in the subHilbert space  $|x\rangle$  ( $|y\rangle$ ). It should be emphasized that in order to generate the  $\pi$ -flux per plaquette, here we have added key phase factors of the translation operator  $V_y$ . By applying the one-step operator in Eq. (3) many times, a multi-step DTQW can be realized, as shown schematically in Fig. 1, and the topological-protected corner states can be explored, as will be shown.

## III. SPECTRA AND TOPOLOGICAL INVARIANT

In order to illustrate the topological features of this DTQW, here we discuss the spectra and the topological invariant. In Fig. 2(a), we plot the quasienergy spectra of the effective Hamiltonian,  $H_{\text{eff}} = i \ln U_{\text{step}}$ , under the open boundary condition. This figure shows clearly that the gapless zero-energy and gapped nonzero-energy states can occur. Moreover, the gapless zero-energy states are four-degenerate and separated from the bulk states by a large energy gap, while these four-degenerate gapped nonzero-energy states are separated from the bulk states only with a tiny gap, as shown in Fig. 2(b). When we increase the parameter  $J_1$ , this tiny bandgap disappears quickly. In Fig. 2(c), we plot the collective distributions of these four-degenerate zero- and nonzero-energy states, which are indeed localized at the

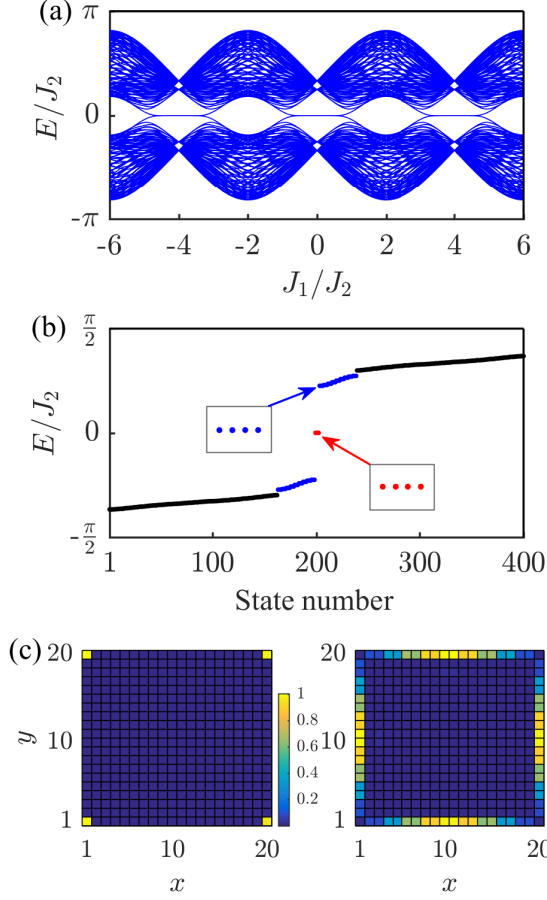


FIG. 2: (a) The quasienergy spectra of the effective Hamiltonian,  $H_{\text{eff}} = i \ln U_{\text{step}}$ , as a function of the parameter  $J_1$ . (b) The quasienergy spectrum with  $J_1 = 0.1$ . There are four-degenerate zero- and nonzero-energy states, denoted respectively by the red and blue points. (c) Left: the collective distribution of the four-degenerate zero-energy corner-localized states. Right: the collective distribution of the four-degenerate nonzero-energy edge-localized states with the state numbers  $\{203, 204, 205, 206\}$ . Here the lattice size is chosen as  $20 \times 20$  and the parameter  $J_2 = 1$ .

four corners and edges of the lattice, respectively.

The appearance of the zero-dimensional corner states can be attributed to the second-order bulk topology, which is described by introducing the Wannier bands and the nested Wilson loops [36, 37]. Generally speaking, the complete characterization of the second-order topology for a Floquet system gives a pair of  $\mathbb{Z}_2$  invariant, which can predict the appearance of zero- and  $\pi$ -corner states [52–56]. For our model, only one  $\mathbb{Z}_2$  invariant is enough with the absence of the  $\pi$ -corner states.

To construct the topological invariant, we consider the eigenstates of the one-step operator in momentum representation

$$U_{\text{step}}(\mathbf{k})|E_{\mathbf{k}}\rangle = e^{-iE_{\mathbf{k}}} |E_{\mathbf{k}}\rangle, \quad (10)$$

where two gapped bands with the quasienergy  $\pm E_{\mathbf{k}}$  are

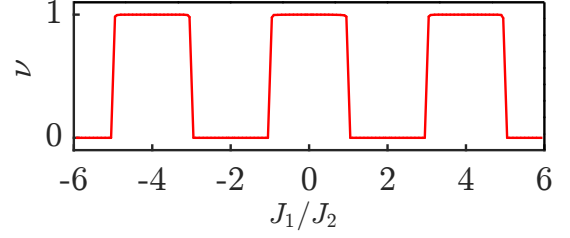


FIG. 3: Numerical plot of the topological invariant  $\nu$  by the nested Wilson loops. The 2D Brillouin zone is discretized by using 51 k-points in each direction.

doubly degenerate, respectively, and the eigenstates can be denoted as  $|+E_{\mathbf{k}}^1\rangle$  and  $|+E_{\mathbf{k}}^2\rangle$  ( $|-E_{\mathbf{k}}^1\rangle$  and  $|-E_{\mathbf{k}}^2\rangle$ ) for upper (lower) bands. When the lower two bands are filled, the Wilson loop operator in the  $x$  direction is defined as

$$\mathcal{W}_{x,\mathbf{k}} = F_{x,\mathbf{k}+(N_x-1)\Delta k_x \mathbf{e}_x} \cdots F_{x,\mathbf{k}+\Delta k_x \mathbf{e}_x} F_{x,\mathbf{k}}, \quad (11)$$

where  $F_{x,\mathbf{k}}$  is a  $2 \times 2$  matrix with element  $[F_{x,\mathbf{k}}]^{mn} = \langle -E_{\mathbf{k}+\Delta k_x \mathbf{e}_x}^m | -E_{\mathbf{k}}^n \rangle$  ( $m, n = 1, 2$ ),  $\mathbf{e}_x$  is the unit vector in the  $x$  direction, and  $\Delta k_x = 2\pi/N_x$ . The 2D Brillouin zone is discretized by using the interval  $(2\pi/N_x, 2\pi/N_y)$ , such that there are  $(N_x + 1)(N_y + 1)$  k-points in total. With the periodic boundary condition,  $|-E_{\mathbf{k}}^n\rangle = |-E_{\mathbf{k}+2\pi \mathbf{e}_x}^n\rangle$ , we diagonalize Eq. (11) as

$$\mathcal{W}_{x,\mathbf{k}} |v_{x,\mathbf{k}}^j\rangle = e^{i2\pi\nu_x^j(k_y)} |v_{x,\mathbf{k}}^j\rangle, \quad (12)$$

where  $j = \pm$  denotes two Wannier bands. These Wannier bands carry their own topological invariants, which can be evaluated by calculating the nested Wilson loops.

We firstly construct the Wannier states as

$$|w_{x,\mathbf{k}}^\pm\rangle = \sum_{n=1,2} [v_{x,\mathbf{k}}^\pm]^n | -E_{\mathbf{k}}^n \rangle, \quad (13)$$

where  $[v_{x,\mathbf{k}}^\pm]^n$  denotes the  $n$ -th element of the 2-component spinor  $|v_{x,\mathbf{k}}^\pm\rangle$ . Then, with the periodic boundary condition,  $|w_{x,\mathbf{k}}^\pm\rangle = |w_{x,\mathbf{k}+2\pi \mathbf{e}_y}^\pm\rangle$ , the nested Wilson loops along  $k_y$  in the Wannier bands  $v_x^\pm$  are

$$\tilde{\mathcal{W}}_{y,\mathbf{k}} = F_{y,\mathbf{k}+(N_y-1)\Delta k_y \mathbf{e}_y}^\pm \cdots F_{y,\mathbf{k}+\Delta k_y \mathbf{e}_y}^\pm F_{y,\mathbf{k}}^\pm, \quad (14)$$

where  $F_{y,\mathbf{k}}^\pm = \langle w_{x,\mathbf{k}+\Delta k_y \mathbf{e}_y}^\pm | w_{x,\mathbf{k}}^\pm \rangle$ ,  $\mathbf{e}_y$  is the unit vector in the  $y$  direction, and  $\Delta k_y = 2\pi/N_y$ . Through Eq. (14), we obtain the nested polarization as

$$p_y^{\nu_x^\pm} = -\frac{i}{2\pi} \frac{1}{N_x} \sum_{k_x} \text{Log}[\tilde{\mathcal{W}}_{y,\mathbf{k}}^\pm]. \quad (15)$$

Similarly, we can also obtain the nested polarization  $p_x^{\nu_y^\pm}$  from the nest Wilson loops in the  $y$  direction. Finally,

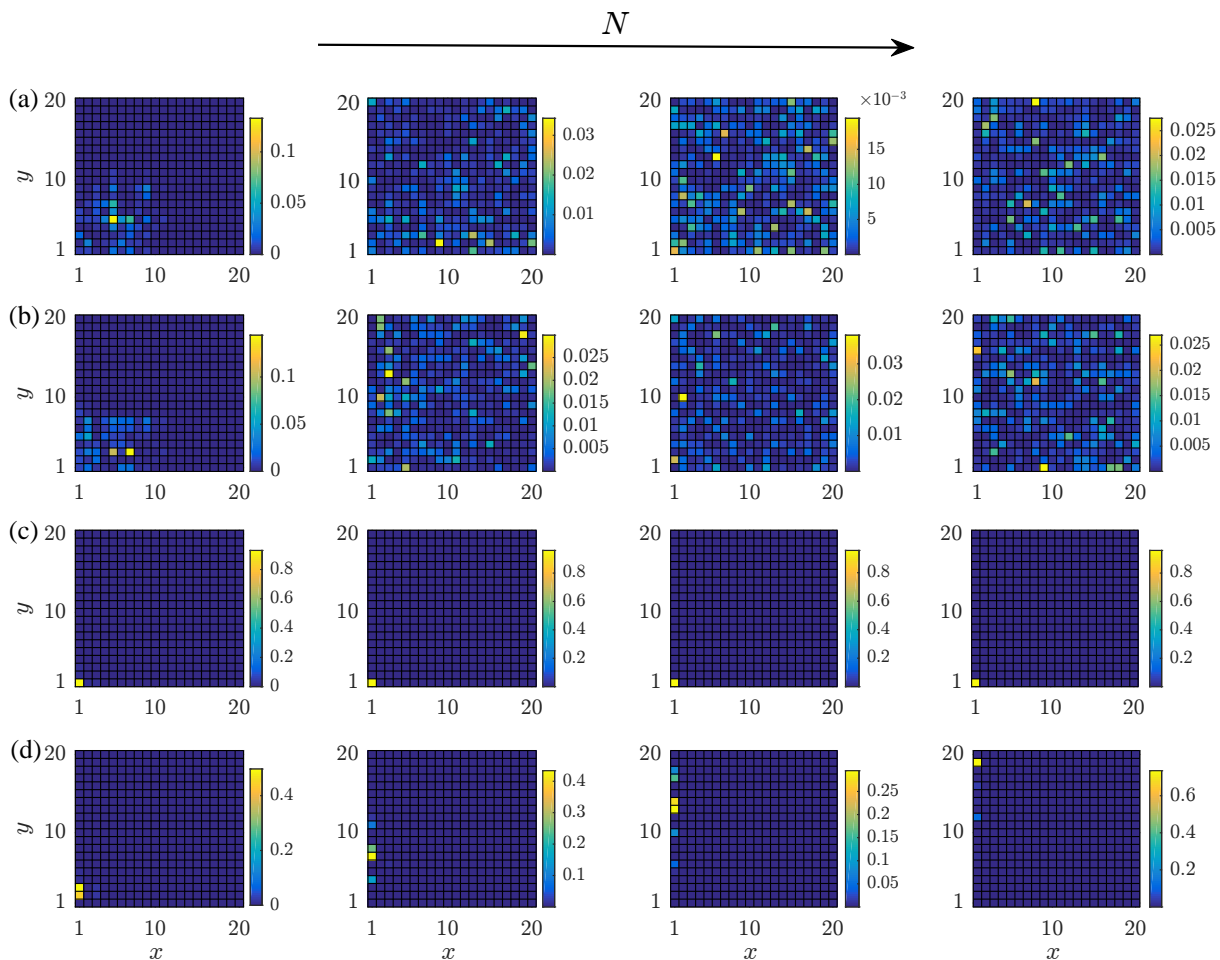


FIG. 4: The probability distributions of the DTQW on a  $20 \times 20$  lattice for subsequent steps of  $N = 5, 50, 100, 150$ . The walker is initialized at one corner  $(x, y) = (1, 1)$  (a,c) or edge  $(x, y) = (1, 2)$  (b,d) of the lattice. In (a,b), the parameter  $J_1 = 1.5$ , which corresponds to a trivial phase. In (c,d), the parameter  $J_1 = 0.1$ , which corresponds to a quadrupole topological phase.

the topological quadrupole phase is characterized by a  $\mathbb{Z}_2$  invariant [36],

$$\nu = 4p_y^{\nu_x^\pm} p_x^{\nu_y^\pm}. \quad (16)$$

By choosing  $N_x = N_y = 50$ , we numerically calculate the topological invariant  $\nu$  by using the above procedure. As shown in Fig. 3, we find that the topological invariant  $\nu$  is quantized to be 0 or 1, which corresponds to the trivial or topological phases, respectively.

#### IV. OBSERVATION OF CORNER AND EDGE STATES

In this section, we mainly show that the corner and edge states can be observed experimentally through the probability distribution of the walker after a multi-step DTQW. It is well known that the probability distributions of multi-step DTQWs exhibit the ballistic behaviors

[1], which are entirely different from the diffusive behaviors of the classic version. Utilizing this feature, we can demonstrate the existence of the corner and edge states through the local behavior of the probability distribution of the walker.

In the first case, we tune the parameter  $J_1 = 1.5$ , which corresponds to a trivial phase. We initialize the walker at one corner of the lattice  $(x, y) = (1, 1)$  or one edge of the lattice with  $(x, y) = (1, 2)$ . Since the system does not support any localized states, the probability of the walker spreads ballistically into the bulk as increasing the number of the DTQW steps; see Figs. 4(a) and 4(b). Then we tune the parameter to  $J_1 = 0.1$ , which corresponds to a quadrupole topological phase supporting the localized corner and edge states; see Fig. 2(c). In such case, when this initial state is prepared at one corner of the lattice  $(x, y) = (1, 1)$ , since it has a large overlap with the corner state, the most part of the walker's wave packet remains localized near  $(x, y) = (1, 1)$  as increasing the step of the DTQW; see Fig. 4(c). In Fig. 4(d), we initialize the walker at one edge of the lattice with  $(x, y) = (1, 2)$ . Sim-

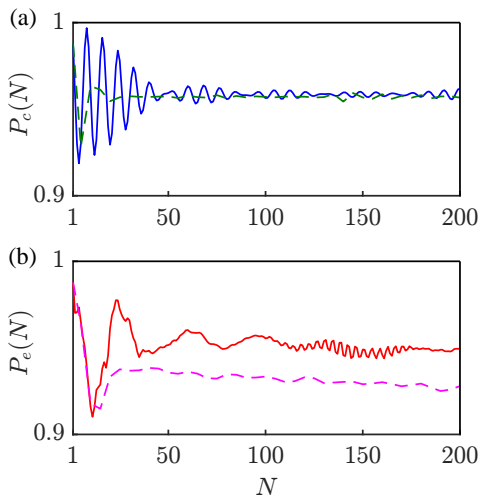


FIG. 5: (a) The probability  $P_c(N)$  at the corner  $(x, y) = (1, 1)$  when the walker is initialized at the same corner. (b) The probability  $P_e(N)$  at the right edge of the lattice when the walker is initialized at  $(x, y) = (1, 2)$ . The parameter  $J_1 = 0.1$ . The solid lines represent the case without the static disorder and the dashed lines represent the case  $W = 2.5$  averaged over the 100 disordered realizations.

ilarly, this initial state has a large overlap with the edge states, and we can also observe a large nonvanishing localization at one edge of the lattice. Since the edge states have a vanishing distribution at the corners of the lattice [see Fig. 2(c)], the walker only localizes at one edge of the lattice.

The observable properties of the corner states are robust against small fluctuations with the second-order topological protection. Conversely, the observable properties of the edge states are not robust due to the tiny gap from the bulk states. To support this claim, we add the static disorder into the evolution processing. The one-step operator for the static disorder is introduced as

$$U_{\text{total}} = U_{\text{step}} \times U_{\text{dis}}, \quad (17)$$

with

$$U_{\text{dis}} = \sum_{x,y} e^{i\delta_{x,y}} |x, y\rangle \langle x, y|. \quad (18)$$

Here  $\delta_{x,y}$  is chosen randomly from the interval  $[-W/2, W/2]$ , where  $W$  is the disorder strength.

Figure 5 shows the probabilities  $P_c(N)$  and  $P_e(N)$  of the walker remained respectively at the corner state or the edge state without and with the static disorder. When the walker is initialized at one corner of the lattice  $(x, y) = (1, 1)$ , it has a stable large probability at this corner as increasing the step of the DTQW, and this corner probability  $P_c(N)$  is robust against the static disorder; see Fig. 5(a). When the walker is initialized at one edge of the lattice  $(x, y) = (1, 2)$ , it also has a large probability at this edge. In Fig. 5(b), we also show that the edge probability  $P_e(N)$  decreases when the static

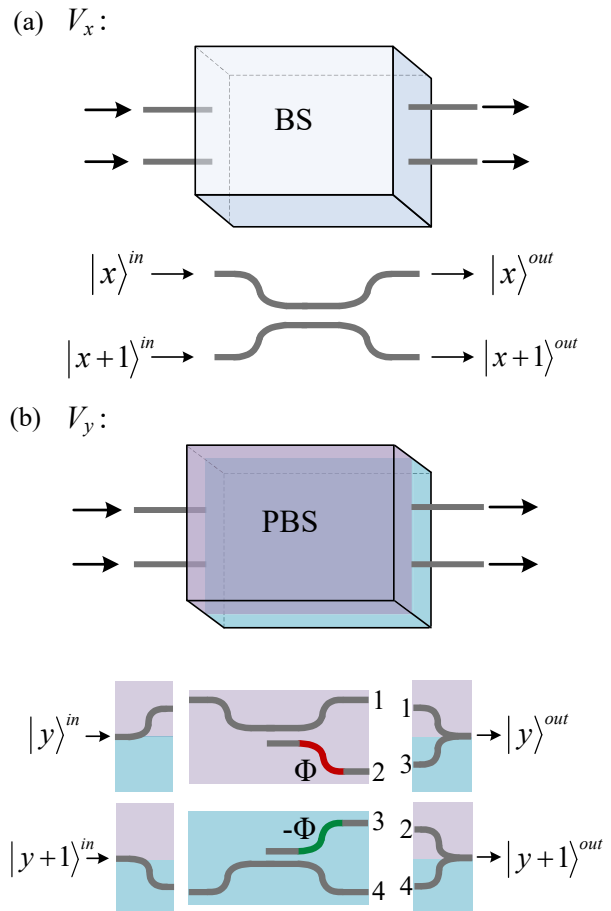


FIG. 6: Scheme of waveguide structure for realizing the translation operators  $V_x$  and  $V_y$ . (a) A single-layer waveguide structure for realizing a beam splitter (BS). (b) A double-layer waveguide structure for realizing a phase-shifted beam splitter (PBS).

disorder is added, demonstrating that the edge states are not robust. This decrease is more evident as we increase the parameter  $J_1$ . The results for other three corners or edges of the lattice are similar and thus not shown here.

## V. POSSIBLE EXPERIMENTAL IMPLEMENTATION

Finally, we propose a possible scheme to realize this DTQW of Eq. (3) in a three-dimensional integrated photonic circuit [57], where a single photon acts as a walker and a single waveguide can indicate a two-dimensional lattice site in the  $x$  and  $y$  directions. The waveguides are extended in the  $z$  direction, corresponding to the time dimension of the DTQW. The key to realize this DTQW in experiments is how to achieve the specific translation operators  $V_x$  and  $V_y$  in Eqs. (8)-(9), which correspond to a beam-splitter matrix and a phased-shifted beam-

splitter matrix, respectively. Fortunately, we can realize these translation operators in an integrated photonic circuit with the directional coupler geometry [58], where two waveguides are brought close together for a certain interaction length and coupled by an evanescent field. In the following, we will show how to implement the translation operators  $V_x$  and  $V_y$  with the single- and double-layer waveguide structures, respectively.

The translation operator  $V_x$  can be realized by a directional coupler; see Fig. 6(a). The standard coupled mode theory [59] gives a transfer matrix as

$$T_1(z) = \begin{pmatrix} \cos(Kz) & -i \sin(Kz) \\ -i \sin(Kz) & \cos(Kz) \end{pmatrix}, \quad (19)$$

which can be used to realize Eq. (8). According to Eq. (19), the parameter in  $V_x$  can be adjusted through altering the coupling coefficient  $K$  and the interaction length  $z$ .

Due to the current technology of full phase-shift controllability between two waveguides [60, 61], we can introduce an arbitrary phase in the first (or second) row of  $T_1(z)$ . However, the phases required in  $V_y$  are at the off-diagonal elements of the matrix, which indicates that we can not realize the translation operator  $V_y$  directly by a single directional coupler. Thus, we design a double-layer waveguide structure to overcome this limitation. As shown in Fig. 6(b), if a single photon pulse is input from the port labeled by  $|y\rangle^{in}$  (or  $|y+1\rangle^{in}$ ), it will go through the upper (or lower) layer waveguide structure and obtain a phase  $\Phi$  (or  $-\Phi$ ). According to the coupled mode theory, the total transfer matrix governed by this double-layer waveguide structure is

$$T_2(z) = \begin{pmatrix} \cos(Kz) & -i \sin(Kz)e^{i\Phi} \\ -i \sin(Kz)e^{-i\Phi} & \cos(Kz) \end{pmatrix}, \quad (20)$$

which is exactly the phased-shifted beam-splitter matrix

in Eq. (9). Thus, the experimental implementation of  $U_{\text{step}}$  is possible with the current technology of the three-dimensional waveguide architecture [62–65]. The phase  $\Phi$  can be chosen arbitrarily and is here taken as  $\Phi = m\pi$ , where  $m$  is an integer. When  $m$  is even, the transfer matrix  $T_2(z)$  reduces to  $T_1(z)$ . That is, a single-layer waveguide structure is enough for this case.

## VI. CONCLUSIONS

In summary, we have constructed a two-dimensional coinless DTQW to simulate the second-order topological insulator. We have shown that both of the corner and edge states can be observed through the probability distribution independently. Furthermore, we have demonstrated the robustness of the topological corner states by introducing the static disorder. Finally, we have proposed a possible experimental implementation in a three-dimensional integrated photonic circuits. Since the coupling and phase between each two lattice sites at each step of DTQWs can be adjusted independently, our scheme can be generalized directly to realize the non-Hermitian [49–51] and Floquet higher-order topological insulators [52–56]. Our work offers a new route to explore exotic higher-order topological matters using DTQWs.

## VII. ACKNOWLEDGMENTS

This work is supported partly by the National Key R&D Program of China under Grant No. 2017YFA0304203; the NSFC under Grant No. 11674200; and 1331KSC.

- 
- [1] Y. Aharonov, L. Davidovich, and N. Zagury, Quantum random walks, *Phys. Rev. A* **48**, 1687 (1993).
  - [2] E. Farhi and S. Gutmann, Quantum computation and decision trees, *Phys. Rev. A* **58**, 915 (1998).
  - [3] J. Kempe, Quantum random walks: An introductory overview, *Contemp. Phys.* **44**, 307327 (2003).
  - [4] A. M. Childs, Universal computation by quantum walk, *Phys. Rev. Lett.* **102**, 180501 (2009).
  - [5] A. M. Childs, D. Gosset, and Z. Webb, Universal computation by multiparticle quantum walk, *Science* **339**, 791 (2013).
  - [6] A. Aspurguzik and P. Walther, Photonic quantum simulators, *Nat. Phys.* **8**, 285 (2012).
  - [7] F. Cardano, F. Massa, H. Qassim, E. Karimi, S. Slusarenko, D. Paparo, C. de Lisio, F. Sciarrino, E. Santamato, R. W. Boyd, and L. Marrucci, Quantum walks and wavepacket dynamics on a lattice with twisted photons, *Sci. Adv.* **1**, e1500087 (2015).
  - [8] O. Boada, L. Novo, F. Sciarrino, and Y. Omar, Quantum walks in synthetic gauge fields with three-dimensional integrated photonics, *Phys. Rev. A* **95**, 013830 (2017).
  - [9] F. Nejdassattari, Y. Zhanf, F. Bouchard, H. Larocque, A. Sit, E. Cohen, R. Fickler, and E. Karimi, Experimental realization of wave-packet dynamics in cyclic quantum walks, *Optica* **6**, 174 (2019).
  - [10] T. Kitagawa, M. S. Rudner, E. Berg, and E. Demler, Exploring topological phases with quantum walks, *Phys. Rev. A* **82**, 033429 (2010).
  - [11] J. K. Asbóth, Symmetries, topological phases, and bound states in the one-dimensional quantum walk, *Phys. Rev. B* **86**, 195414 (2012).
  - [12] J. K. Asbóth and H. Obuse, Bulk-boundary correspondence for chiral symmetric quantum walks, *Phys. Rev. B* **88**, 121406 (2013).
  - [13] H. Obuse, J. K. Asbóth, Y. Nishimura, and N. Kawakami, Unveiling hidden topological phases of a one-

- dimensional Hadamard quantum walk, *Phys. Rev. B* **92**, 045424 (2015).
- [14] J. M. Edge and J. K. Asbóth, Localization, delocalization, and topological transitions in disordered two-dimensional quantum walks, *Phys. Rev. B* **91**, 104202 (2015).
- [15] T. Rakovszky and J. K. Asbóth, Localization, delocalization, and topological phase transitions in the one-dimensional split-step quantum walk, *Phys. Rev. A* **92**, 052311 (2015).
- [16] T. Groh, S. Brakhane, W. Alt, D. Meschede, J. K. Asbóth, and A. Alberti, Robustness of topologically protected edge states in quantum walk experiments with neutral atoms, *Phys. Rev. A* **94**, 013620 (2016).
- [17] T. Rakovszky, J. K. Asbóth, and A. Alberti, Detecting topological invariants in chiral symmetric insulators via losses, *Phys. Rev. B* **95**, 201407 (2017).
- [18] V. V. Ramasesh, E. Flurin, M. Rudner, I. Siddiqi, and N. Y. Yao, Direct probe of topological invariants using Bloch oscillating quantum walks, *Phys. Rev. Lett.* **118**, 130501 (2017).
- [19] M. Sajid, J. K. Asbóth, D. Meschede, R. F. Werner, and A. Alberti, Creating anomalous Floquet Chern insulators with magnetic quantum walks, *Phys. Rev. B* **99**, 214303 (2019).
- [20] T. Kitagawa, M. A. Broome, A. Fedrizzi, M. S. Rudner, E. Berg, I. Kassal, A. Aspuru-Guzik, E. Demler, and A. G. White, Observation of topologically protected bound states in photonic quantum walks, *Nat. Commun.* **3**, 882 (2012).
- [21] F. Cardano, M. Maffei, F. Massa, B. Piccirillo, C. de Lisio, G. De Filippis, V. Cataudella, E. Santamato, and L. Marrucci, Statistical moments of quantum-walk dynamics reveal topological quantum transitions, *Nat. Commun.* **7**, 11439 (2016).
- [22] F. Cardano, A. D'Errico, A. Dauphin, M. Maffei, B. Piccirillo, C. D. Lisio, G. D. Filippis, V. Cataudella, E. Santamato, L. Marrucci, M. Lewenstein, and P. Massignan, Detection of Zak phases and topological invariants in a chiral quantum walk of twisted photons, *Nat. Commun.* **8**, 15516 (2017).
- [23] E. Flurin, V. V. Ramasesh, S. Hacoheh-Gourgy, L. S. Martin, N. Y. Yao, and I. Siddiqi, Observing topological invariants using quantum walks in superconducting circuits, *Phys. Rev. X* **7**, 031023 (2017).
- [24] X.-Y. Xu, Q.-Q. Wang, W.-W. Pan, K. Sun, J.-S. Xu, G. Chen, J.-S. Tang, M. Gong, Y.-J. Han, C.-F. Li, and G.-C. Guo, Measuring the winding number in a large-scale chiral quantum walk, *Phys. Rev. Lett.* **120**, 260501 (2018).
- [25] H. Chalabi, S. Barik, S. Mittal, T. E. Murphy, M. Hafezi, and E. Waks, Synthetic gauge field for two-dimensional time-multiplexed quantum random walks, *Phys. Rev. Lett.* **123**, 150503 (2019).
- [26] D.-Z. Xie, T.-S. Deng, T. Xiao, W. Gou, T. Chen, W. Yi, and B. Yan, Topological quantum walks in momentum space with a Bose-Einstein condensate, *Phys. Rev. Lett.* **124**, 050502 (2020).
- [27] L. Xiao, X. Zhan, Z.-H. Bian, K.-K. Wang, X. Zhang, X.-P. Wang, J. Li, K. Mochizuki, D. Kim, N. Kawakami, W. Yi, H. Obuse, B. C. Sanders, and P. Xue, Observation of topological edge states in parity-time-symmetric quantum walks, *Nat. Phys.* **13**, 1117 (2017).
- [28] X. Zhan, L. Xiao, Z.-H. Bian, K.-K. Wang, X.-Z. Qiu, B. C. Sanders, W. Yi, and P. Xue, Detecting topological invariants in nonunitary discrete-time quantum walks, *Phys. Rev. Lett.* **119**, 130501 (2017).
- [29] K.-K. Wang, X.-Z. Qiu, L. Xiao, X. Zhan, Z.-H. Bian, B. C. Sanders, W. Yi, and P. Xue, Observation of emergent momentum-time skyrmions in parity-time-symmetric non-unitary quench dynamics, *Nat. Commun.* **10**, 2293 (2019).
- [30] K.-K. Wang, X.-Z. Qiu, L. Xiao, X. Zhan, Z.-H. Bian, W. Yi, and P. Xue, Simulating dynamic quantum phase transitions in photonic quantum walks, *Phys. Rev. Lett.* **122**, 020501 (2019).
- [31] L. Xiao, K.-K. Wang, X. Zhan, Z.-H. Bian, K. Kawabata, M. Ueda, W. Yi, and P. Xue, Observation of critical phenomena in parity-time-symmetric quantum dynamics, *Phys. Rev. Lett.* **123**, 230401 (2019).
- [32] B. Wang, T. Chen, and X. Zhang, Experimental observation of topologically protected bound states with vanishing Chern numbers in a two-dimensional quantum walk, *Phys. Rev. Lett.* **121**, 100501 (2018).
- [33] C. Chen, X. Ding, J. Qin, Y. He, Y. Luo, M. Chen, C. Liu, X. Wang, W. Zhang, H. Li, L. You, Z. Wang, D. Wang, B. C. Sanders, C. Lu, and J. Pan, Observation of topologically protected edge states in a photonic two-dimensional quantum walk, *Phys. Rev. Lett.* **121**, 100502 (2018).
- [34] H. Chalabi, S. Barik, S. Mittal, T. E. Murphy, M. Hafezi, and E. Waks, Synthetic gauge field for two-dimensional time-multiplexed quantum random walks, *Phys. Rev. Lett.* **123**, 150503 (2019).
- [35] A. D'Errico, F. Cardano, M. Maffei, A. Dauphin, R. Barboza, C. Esposito, B. Piccirillo, M. Lewenstein, P. Massignan, and L. Marrucci, Two-dimensional topological quantum walks in the momentum space of structured light, *Optica* **7**, 108 (2020).
- [36] W. A. Benalcazar, B. A. Bernevig, and T. L. Hughes, Quantized electric multipole insulators, *Science* **357**, 61 (2017).
- [37] W. A. Benalcazar, B. A. Bernevig, and T. L. Hughes, Electric multiple moments, topological multipolemoment pumping, and chiral hinge states in crystalline insulators, *Phys. Rev. B* **96**, 245115 (2017).
- [38] J. Langbehn, Y. Peng, L. Trifunovic, F. von Oppen, and P. W. Brouwer, Reflection-symmetric second-order topological insulators and superconductors, *Phys. Rev. Lett.* **119**, 246401 (2017).
- [39] Z. Song, Z. Fang, and C. Fang, (d-2)-dimensional edge states of rotation symmetry protected topological states, *Phys. Rev. Lett.* **119**, 246402 (2017).
- [40] F. Schindler, A. M. Cook, M. G. Vergniory, Z. Wang, S. S. P. Parkin, B. A. Bernevig, and T. Neupert, Higher-order topological insulators, *Sci. Adv.* **4**, eaat0346 (2018).
- [41] M. Serra-Garcia, V. Peri, R. Süsstrunk, O. R. Bilal, T. Larsen, L. G. Villanueva, and S. D. Huber, Observation of a phononic quadrupole topological insulator, *Nature (London)* **555**, 342 (2018).
- [42] C. W. Peterson, W. A. Benalcazar, T. L. Hughes, and G. Bahl, A quantized microwave quadrupole insulator with topologically protected corner states, *Nature (London)* **555**, 346 (2018).
- [43] F. Schindler, Z.-J. Wang, M. G. Vergniory, A. M. Cook, A. Murani, S. Sengupta, A. Y. Kasumov, R. Deblock, S. Jeon, I. Drozdov, H. Bouchiat, S. Guéron, A. Yazdani, B. A. Bernevig, and T. Neupert, Higher-order topology

- in bismuth, *Nat. Phys.* **14**, 918 (2018).
- [44] S. Imhof, C. Berger, F. Bayer, J. Brehm, L. Molenkamp, T. Kiessling, F. Schindler, C. H. Lee, M. Greiter, T. Neupert, and R. Thomale, Topological-circuit realization of topological corner modes, *Nat. Phys.* **14**, 925 (2018).
- [45] S. Mittal, V. V. Orre, G. Zhu, M. A. Gorlach, A. Poddubny, and M. Hafezi, Photonic quadrupole topological phases, *Nat. Phys.* **13**, 692 (2019).
- [46] F. Zangeneh-Nejad and R. Fleury, Nonlinear second-order topological insulators, *Phys. Rev. Lett.* **123**, 093502 (2019).
- [47] Y. You, D. Litinski and F. von Oppen, Higher-order topological superconductors as generators of quantum codes, *Phys. Rev. B* **100**, 054513 (2019).
- [48] K. Laubscher, D. Loss, and J. Klinovaja, Fractional topological superconductivity and parafermion corner states, *Phys. Rev. Research* **1**, 032017 (2019).
- [49] C. H. Lee, L. Li, and J. Gong, Hybrid higher-order skin-topological modes in nonreciprocal systems, *Phys. Rev. Lett.* **123**, 016805 (2019).
- [50] T. Liu, Y.-R. Zhang, Q. Ai, Z. Gong, K. Kawabata, M. Ueda, and F. Nori, Second-order topological phases in non-Hermitian systems, *Phys. Rev. Lett.* **122**, 076801 (2019).
- [51] X.-W. Luo and C.-W. Zhang, Higher-order topological corner states induced by gain and loss, *Phys. Rev. Lett.* **123**, 073601 (2019).
- [52] M. Rodriguez-Vega, A. Kumar, and B. Seradjeh, Higher-order Floquet topological phases with corner and bulk bound states, *Phys. Rev. B* **100**, 085138 (2019).
- [53] R. W. Bomantara, L. Zhou, J. Pan, and J. Gong, Coupled-wire construction of static and Floquet second-order topological insulators, *Phys. Rev. B* **99**, 045441 (2019).
- [54] R. Seshadri, A. Dutta, and D. Sen, Generating a second-order topological insulator with multiple corner states by periodic driving, *Phys. Rev. B* **100**, 115403 (2019).
- [55] Y. Peng and G. Refael, Floquet second-order topological insulators from nonsymmorphic space-time symmetries, *Phys. Rev. Lett.* **123**, 016806 (2019).
- [56] H. Hu, B. Huang, E. Zhao, and W. Vincent Liu, Dynamical singularities of Floquet higher-order topological insulators, *Phys. Rev. Lett.* **124**, 057001 (2020).
- [57] S. Gross and M. J. Withford, Ultrafast-laser-inscribed 3D integrated photonics: challenges and emerging applications, *Nanophotonics* **4**, 332 (2015).
- [58] F. Flamini, N. Spagnolo, and F. Sciarrino, Two-particle bosonic-fermionic quantum walk via integrated photonics, *Phys. Rev. Lett.* **108**, 010502 (2012).
- [59] K. Okamoto, *Fundamentals and applications of optical waveguides* (Elsevier, San Diego, 2006).
- [60] A. Crespi, R. Osellame, R. Ramponi, D. J. Brod, E. F. Galvão, N. Spagnolo, C. Vitelli, E. Maiorino, P. Mataloni, and F. Sciarrino, Integrated multimode interferometers with arbitrary designs for photonic boson sampling, *Nat. Photonics* **7**, 545 (2013).
- [61] A. Crespi, R. Osellame, R. Ramponi, V. Giovannetti, R. Fazio, L. Sansoni, F. D. Nicola, F. Sciarrino, and P. Mataloni, Anderson localization of entangled photons in an integrated quantum walk, *Nat. Photonics* **7**, 322 (2013).
- [62] S. Nolte, M. Will, J. Burghoff, and A. Tuennermann, Femtosecond waveguide writing: a new avenue to three-dimensional integrated optics, *Appl. Phys. A Mater. Sci. Process.* **77**, 109 (2003).
- [63] N. Spagnolo, C. Vitelli, L. Sansoni, E. Maiorino, P. Mataloni, F. Sciarrino, D. J. Brod, E. F. Galvão, A. Crespi, R. Ramponi, and R. Osellame, General rules for bosonic bunching in multimode interferometers, *Phys. Rev. Lett.* **111**, 130503 (2013).
- [64] H. Tang, X.-F. Lin, Z. Feng, J.-Y. Chen, J. Gao, K. Sun, C.-Y. Wang, P.-C. Lai, X.-Y. Xu, Y. Wang, L.-F. Qiao, A.-L. Yang, and X.-M. Jin, Experimental two-dimensional quantum walk on a photonic chip, *Sci. Adv.* **4**, eaat3174 (2018).
- [65] H. Tang, C. D. Franco, Z.-Y. Shi, T.-S. He, Z. Feng, J. Gao, K. Sun, Z.-M. Li, Z.-Q. Jiao, T.-Y. Wang, M. S. Kim, and X.-M. Jin, Experimental quantum fast hitting on hexagonal graphs, *Nat. Photonics* **12**, 754 (2018).